JOURNAL OF Applied Polymer SCIENCE

Special Issue: Microfiltration and Ultrafiltration Membrane Science and Technology

Guest Editors: Prof. Isabel C. Escobar (University of Toledo) and Prof. Bart Van der Bruggen (University of Leuven)

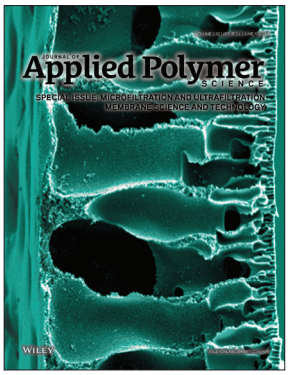

EDITORIAL

Microfiltration and Ultrafiltration Membrane Science and Technology
I. C. Escobar and B. Van der Bruggen, *J. Appl. Polym. Sci.* 2015, **DOI: 10.1002/app.42002**

REVIEWS

Nanoporous membranes generated from self-assembled block polymer precursors: *Quo Vadis*?
Y. Zhang, J. L. Sargent, B. W. Boudouris and W. A. Phillip, *J. Appl. Polym. Sci.* 2015, **DOI: 10.1002/app.41683**

Making polymeric membranes anti-fouling via "grafting from" polymerization of zwitterions
Q. Li, J. Imbrogno, G. Belfort and X.-L. Wang, *J. Appl. Polym. Sci.* 2015, **DOI: 10.1002/app.41781**

Fouling control on MF/ UF membranes: Effect of morphology, hydrophilicity and charge
R. Kumar and A. F. Ismail, *J. Appl. Polym. Sci.* 2015, **DOI: 10.1002/app.42042**

EMERGING MATERIALS AND FABRICATION

Preparation of a poly(phthalazine ether sulfone ketone) membrane with propanedioic acid as an additive and the prediction of its structure
P. Qin, A. Liu and C. Chen, *J. Appl. Polym. Sci.* 2015, **DOI: 10.1002/app.41621**

Preparation and characterization of MOF-PES ultrafiltration membranes
L. Zhai, G. Li, Y. Xu, M. Xiao, S. Wang and Y. Meng, *J. Appl. Polym. Sci.* 2015, **DOI: 10.1002/app.41663**

Tailoring of structures and permeation properties of asymmetric nanocomposite cellulose acetate/silver membranes
A. S. Figueiredo, M. G. Sánchez-Loredo, A. Maurício, M. F. C. Pereira, M. Minhalma and M. N. de Pinho, *J. Appl. Polym. Sci.* 2015, **DOI: 10.1002/app.41796**

LOW-FOULING POLYMERS

Low fouling polysulfone ultrafiltration membrane via click chemistry
Y. Xie, R. Tayouo and S. P. Nunes, *J. Appl. Polym. Sci.* 2015, **DOI: 10.1002/app.41549**

Elucidating membrane surface properties for preventing fouling of bioreactor membranes by surfactin
N. Behary, D. Lecouturier, A. Perwuelz and P. Dhulster, *J. Appl. Polym. Sci.* 2015, **DOI: 10.1002/app.41622**

PVC and PES-*g*-PEGMA blend membranes with improved ultrafiltration performance and fouling resistance
S. Jiang, J. Wang, J. Wu and Y. Chen, *J. Appl. Polym. Sci.* 2015, **DOI: 10.1002/app.41726**

Improved antifouling properties of TiO_2/PVDF nanocomposite membranes in UV coupled ultrafiltration
M. T. Moghadam, G. Lesage, T. Mohammadi, J.-P. Mericq, J. Mendret, M. Heran, C. Faur, S. Brosillon, M. Hemmati and F. Naeimpoor, *J. Appl. Polym. Sci.* 2015, **DOI: 10.1002/app.41731**

Development of functionalized doped carbon nanotube/polysulfone nanofiltration membranes for fouling control
P. Xie, Y. Li and J. Qiu, *J. Appl. Polym. Sci.* 2015, **DOI: 10.1002/app.41835**

JOURNAL OF Applied Polymer SCIENCE

Special Issue: Microfiltration and Ultrafiltration Membrane Science and Technology

Guest Editors: Prof. Isabel C. Escobar (University of Toledo) and
Prof. Bart Van der Bruggen (University of Leuven)

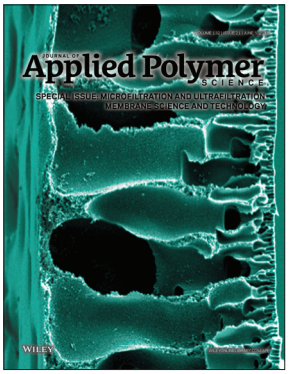

SURFACE MODIFICATION OF POLYMER MEMBRANES

Highly chlorine and oily fouling tolerant membrane surface modifications by *in situ* polymerization of dopamine and poly(ethylene glycol) diacrylate for water treatment
K. Yokwana, N. Gumbi, F. Adams, S. Mhlanga, E. Nxumalo and B. Mamba, *J. Appl. Polym. Sci.* 2015, **DOI: 10.1002/app.41661**

Fouling control through the hydrophilic surface modification of poly(vinylidene fluoride) membranes
H. Jang, D.-H. Song, I.-C. Kim, and Y.-N. Kwon, *J. Appl. Polym. Sci.* 2015, **DOI: 10.1002/app.41712**

Hydroxyl functionalized PVDF-TiO_2 ultrafiltration membrane and its antifouling properties
Y. H. Teow, A. A. Latif, J. K. Lim, H. P. Ngang, L. Y. Susan and B. S. Ooi, *J. Appl. Polym. Sci.* 2015, **DOI: 10.1002/app.41844**

Enhancing the antifouling properties of polysulfone ultrafiltration membranes by the grafting of poly(ethylene glycol) derivatives via surface amidation reactions
H. Yu, Y. Cao, G. Kang, Z. Liu, W. Kuang, J. Liu and M. Zhou, *J. Appl. Polym. Sci.* 2015, **DOI: 10.1002/app.41870**

SEPARATION APPLICATIONS

Experiment and simulation of the simultaneous removal of organic and inorganic contaminants by micellar enhanced ultrafiltration with mixed micelles
A. D. Vibhandik, S. Pawar and K. V. Marathe, *J. Appl. Polym. Sci.* 2015, **DOI: 10.1002/app.41435**

Polymeric membrane modification using SPEEK and bentonite for ultrafiltration of dairy wastewater
A. Pagidi, Y. Lukka Thuyavan, G. Arthanareeswaran, A. F. Ismail, J. Jaafar and D. Paul, *J. Appl. Polym. Sci.* 2015, **DOI: 10.1002/app.41651**

Forensic analysis of degraded polypropylene hollow fibers utilized in microfiltration
X. Lu, P. Shah, S. Maruf, S. Ortiz, T. Hoffard and J. Pellegrino, *J. Appl. Polym. Sci.* 2015, **DOI: 10.1002/app.41553**

A surface-renewal model for constant flux cross-flow microfiltration
S. Jiang and S. G. Chatterjee, *J. Appl. Polym. Sci.* 2015, **DOI: 10.1002/app.41778**

Ultrafiltration of aquatic humic substances through magnetically responsive polysulfone membranes
N. A. Azmi, Q. H. Ng and S. C. Low, *J. Appl. Polym. Sci.* 2015, **DOI: 10.1002/app.41874**

BIOSEPARATIONS APPLICATIONS

Analysis of the effects of electrostatic interactions on protein transport through zwitterionic ultrafiltration membranes using protein charge ladders
M. Hadidi and A. L. Zydney, *J. Appl. Polym. Sci.* 2015, **DOI: 10.1002/app.41540**

Modification of microfiltration membranes by hydrogel impregnation for pDNA purification
P. H. Castilho, T. R. Correia, M. T. Pessoa de Amorim, I. C. Escobar, J. A. Queiroz, I. J. Correia and A. M. Morão, *J. Appl. Polym. Sci.* 2015, **DOI: 10.1002/app.41610**

Hemodialysis membrane surface chemistry as a barrier to lipopolysaccharide transfer
B. Madsen, D. W. Britt, C.-H. Ho, M. Henrie, C. Ford, E. Stroup, B. Maltby, D. Olmstead and M. Andersen, *J. Appl. Polym. Sci.* 2015, **DOI: 10.1002/app.41550**

Membrane adsorbers comprising grafted glycopolymers for targeted lectin binding
H. C. S. Chenette and S. M. Husson, *J. Appl. Polym. Sci.* 2015, **DOI: 10.1002/app.41437**

Journal of Applied Polymer Science

Poly(vinyl chloride) and poly(ether sulfone)-*g*-poly(ether glycol) methyl ether methacrylate blend membranes with improved ultrafiltration performance and fouling resistance

Shuhong Jiang, Jun Wang, Jun Wu, Yinchuan Chen
College of Environmental Science and Engineering, Donghua University, Shanghai 201620, China
Correspondence to: J. Wang (E-mail: wangj@dhu.edu.cn)

ABSTRACT: To enhance the permeability, hydrophilicity, and antifouling properties of poly(vinyl chloride) (PVC) membranes, in this study, poly(ether glycol) methyl ether methacrylate (PEGMA) was grafted onto poly(ether sulfone) (PES) to first synthesize PES-*g*-PEGMA. Then, PES-*g*-PEGMA was blended with PVC (with blend ratios of PVC/PES-*g*-PEGMA that varied from 10 : 0 to 7 : 3) through the non-solvent-induced phase separation method to fabricate PVC/PES-*g*-PEGMA blend membranes. Shear viscosity and Fourier transform infrared–attenuated total reflection experiments showed that PVC/PES-*g*-PEGMA was a partially compatible system and that it was more compatible than a PVC/PES blending system. The contact angle, equilibrium water content, and X-ray photoelectron spectroscopy measurements confirmed that the PVC/PES-*g*-PEGMA blend membranes had a stronger hydrophilicity than the pure PVC membranes. Additionally, the results of this experiment also show that the PVC/PES-*g*-PEGMA blend membranes exhibited a higher permeability and superior antifouling properties than the pure PVC membranes, and the optimum blend ratio of the PVC/PES-*g*-PEGMA blend membranes was 7 : 3. © 2014 Wiley Periodicals, Inc. J. Appl. Polym. Sci. **2015**, *132*, 41726.

KEYWORDS: blends; grafting; membranes; poly(vinyl chloride)

Received 13 June 2014; accepted 31 October 2014
DOI: 10.1002/app.41726

INTRODUCTION

Water pollution is becoming a serious environmental issue that impacts the survival of mankind. Consequently, more stringent regulations and the extensive treatment of wastewater are becoming increasingly important. One of the latest trends in wastewater treatment is the application of membrane separation technologies, which have been gradually applied in industry.[1–5] A common characteristic of wastewater is a high quantity of complicated components, such as proteins, polysaccharides, and dissolved organic matter.[6,7] These components tend to result in serious fouling of hydrophobic membranes, but for hydrophilic membranes, the fouling is weaker. Membrane fouling sharply decreases the water flux and increases the frequency of backwashing, so the lifetime of membranes is impaired. This not only seriously hinders the working efficiency of the membranes but also results in rising costs. Therefore, the membranes used in wastewater treatment should be hydrophilic and have a low cost. Additionally, they should also possess a high water flux and separation efficiency. However, current commercial membranes usually possess a strong hydrophobicity, so research into and the development of highly hydrophilic, highly permeable, and cost-effective membranes is needed.[8–11]

Poly(vinyl chloride) (PVC), as the second largest composite resin in industry, has the advantages of abrasion resistance, acid and alkali resistance, chemical performance stabilization, innocuous nature, and low cost. Therefore, it has been widely used in traditional membrane technology processes, such as water/wastewater treatment, reverse osmosis pretreatment, and separation, and in the textile, chemical, and biochemical industries. However, PVC membranes are inclined to be fouled because of their strong hydrophobicity, so the use of PVC as a membrane material is still greatly limited. To improve PVC membrane's antifouling properties through the enhancement of the surface hydrophilicity, many techniques have been used to modify PVC membranes; these include coating,[12] polymer blending,[13–17] plasma treatment,[18] and surface grafting.[19–21] Among these methods, polymer blending is valuable because it is the least expensive, the most convenient in operation, and the most versatile way of achieving materials with new, desirable properties.[22] Some researchers have investigated blending systems in which PVC is combined with other polymers. For example, Peng and Sui[15] reported the performance of PVC blended with poly(vinyl butyral), and the results show that the water flux and hydrophilicity of the blend membranes were much better than that of pure PVC membranes. Mei *et al.*[16] proposed the interfacial hydrolysis of polyacrylonitrile

between PVC and SiO_2 to improve the hydrophilicity and permeability of PVC/polyacrylonitrile/SiO_2 composite hollow-fiber membranes. The results indicate that both the water permeation and antifouling performance were improved, whereas the mechanical strength was maintained at a high level.

Because of its favorable mechanical properties and thermooxidative stability, poly(ether sulfone) (PES) is widely used in membrane preparation for various applications. However, the hydrophobicity and high price of PES limit its applications in wastewater treatment. Consequently, many researchers have been engaged in the improvement of the PES membrane hydrophilicity by chemical methods or by blending with other materials, such as polyvinylidene fluoride (PVDF), cellulose acetate phthalate (CAP), and so on.[23–26] The method of the hydrophilic modification of PES that is most commonly reported in the literature is grafting. In particular, the grafting of a hydrophilic monomer onto hydrophobic polymers offers an effective approach for improving the hydrophilicity of the parent polymer. For instance, Shi *et al.*[27] found that grafting methacrylic acid onto PES using benzoyl peroxide (BPO) as a chemical initiator could not only increase the hydrophilicity of PES membranes but also endow the membranes with distinct pH sensitivity. Yune *et al.*[28] reported that in the use of photoinduced graft polymerization with a recently developed high-throughput platform to graft poly(ethylene glycol) methyl ether methacrylate (PEG) onto PES membranes, the antifouling properties of the PEG-grafted PES membranes were far better than those of commercial PES membranes. However, in the grafting of poly(ether glycol) methyl ether methacrylate (PEGMA) onto PES to synthesize PES-*g*-PEGMA and then blends with PVC, research into the PVC/PES-*g*-PEGMA blending system has not yet been reported.

In this study, the hydrophilicity, permeability, and antifouling properties of PVC membranes were investigated when they were blended with PES-*g*-PEGMA. PVC/PES-*g*-PEGMA blend membranes were prepared by the non-solvent-induced phase separation (NIPS) method. The objective of this study was to improve the hydrophilicity, water flux, and antifouling performance of PVC membranes for wastewater treatment. The effects of the PES-*g*-PEGMA concentration on the properties of the PVC membranes were also investigated. To sufficiently demonstrate the excellent performance of the PVC/PES-*g*-PEGMA blend membranes, the compatibility, morphology, water flux, and rejection of the PVC/PES-*g*-PEGMA blend membranes were compared with those of PVC/PES blend membranes.

EXPERIMENTAL

Materials

PES in flake form [6020P, weight-average molecular weight (M_w) = 59,000] was provided by BASF Co. (Germany) and dried at 100°C for 24 h before use. Poly(ether glycol) methyl ether methacrylate (PEGMA) monomers [$(PEG)_{4.5}$MA with a number-average molecular weight of 300] was purchased from Sigma-Aldrich Co. BPO and bovine serum albumin (BSA; M_w = 67,000) were purchased from Sinopharm Chemical Reagent (China). PVC was produced by the Chlor-Alkali Chemical Co. (China). *N*,*N*-Dimethylacetamide (DMAC) was purchased from Ling Feng Chemical Reagent Co. (China).

Instruments

The following method and instrumentation were used in this study: a Fourier transform infrared (FTIR)–attenuated total reflection (ATR) spectrometer (TENSOR37, Bruker, Germany), rotating viscometer (DNJ-1, Jinghai, China), total organic carbon analyzer (TOC-VCPN, Shimadzu, Japan), contact angle meter (SL200C, Solon, China), moisture analyzer (DHS-16A, Qinghai, China), freeze dryer (Heto PowerDry LL 3000, Gene), X-ray photoelectron spectroscopy (XPS; PHI), scanning electron microscopy (SEM; JSM-5600LV, Japan), field emission scanning electron microscopy (FESEM; S-4800, HITACHI, Japan), material testing machine (H5K-S, United Kingdom), and filtration cell (MSC300, China).

Synthesis of PES-*g*-PEGMA

The PES-*g*-PEGMA was synthesized as follows. First, 80 g of PES flakes was introduced into a three-necked flask with 480 mL of deionized water, and then, a steady stream of nitrogen was injected into the mixture for 20 min to remove oxygen before 0.5 wt % BPO was added. After 30 min of initiation, 320 mL of aqueous solution containing specific amounts of PEGMA was added dropwise into the reaction vessel. The polymerization was carried out under a nitrogen atmosphere for 2 h, and the temperature was kept constant with a water bath at 70°C for the entire duration of the reaction. The polymer product was dipped in absolute ethyl alcohol for 24 h and then washed sufficiently with hot water. The remaining grafted PES flakes were collected and dried in an oven at 80°C until they reached a constant weight. The graft yield (GY) was calculated gravimetrically according to eq. (1):[27,29,30]

$$GY = \frac{W_f - W_i}{W_i} \quad (1)$$

where W_f is the weight of grafted PES flakes (g) and W_i is the initial PES weight (g).

To confirm the successful polymerization of PEGMA onto PES, the PES-*g*-PEGMA was studied by FTIR–ATR spectroscopy (TENSOR37, Bruker, Germany).

Compatibility Study of the Blending System

The compatibility of the blending system was estimated by shear viscosity and FTIR–ATR measurements.

The shear viscosities of the solutions with different blend ratios of PVC/PES-*g*-PEGMA and PVC/PES were measured in a rotating viscometer (DNJ-1, Jinghai, China). The measurements were performed at room temperature and at a constant shear rate.

FTIR–ATR spectroscopy was used as one way to estimate the compatibility of the PVC/PES-*g*-PEGMA and PVC/PES blending systems. The casting polymer solutions were prepared by the dissolution of the polymers in DMAC at various PVC/PES-*g*-PEGMA and PVC/PES blend ratios. The samples were placed in the sample holder, and all of the spectra were recorded across the wave-number range 4000–650 cm^{-1} by the accumulation of 32 scans at a resolution of 2 cm^{-1}.

Preparation of the Blend Membranes

Flat-sheet porous PVC/PES-*g*-PEGMA (GY = 5.4%) and PVC/PES membranes were prepared by the NIPS method. Certain

ratios of blending systems were dissolved in DMAC with a polymer concentration of 15% (w/w) and stirred at 80°C for approximately 7 h to form a homogeneous solution. The casting solution was filtered and then evacuated to remove any undissolved residuals and air bubbles. The homogeneous solution was then cast on a glass plate and immediately immersed in a deionized water bath maintained at room temperature. The film was peeled off and leached overnight in water to completely remove any traces of solvent. Then, the film was kept in a 50 wt % glycerol aqueous solution for 24 h to prevent the collapse of the porous structure. The wet membranes were directly used for permeability and fouling resistance measurements after the remaining diluents were extracted by thorough washing with deionized water. The dry membranes were freeze-dried (Heto PowerDry LL 3000, Gene) and stored for testing.

Characterization of the Blend Membranes

Microscopic Observation. The cross section and surface morphologies of the blend membranes were observed by SEM (JSM-5600LV, Japan) and FESEM (S-4800, Hitachi, Japan). The membranes were frozen in liquid nitrogen, broken, and sputtered with gold before SEM analysis.

Permeability and Rejection of the Blend Membranes. The membrane permeability properties were tested in an ultrafiltration (UF) laboratory unit at a pressure of 0.10 MPa and room temperature. The system consisted of a filtration cell (MSC300, China) with a volume capacity of 300 mL and a filter area of 37.37 cm^2. The feed side of the system was pressed by air.

After the membrane was fixed, the stirred cell and solution reservoir were fed with distilled water. Each membrane was initially pressurized until there was no further variation in the permeate flux for 300 min at 0.10 MPa before use. The water flux was calculated by the measurement of the filter time at a fixed volume under a constant transmembrane pressure. The water flux (J_{w1}; L $m^{-2}{\cdot}h^{-1}$) was calculated with the following eq. (2):

$$J_{w1}=\frac{V}{At} \tag{2}$$

where V, A, and t represent the volume of permeated water (L), the membrane filtering area (m^2), and the permeation time (h), respectively.

The same unit was fed with a 1.0 mg/mL BSA (molecular weight = 67,000) solution for the rejection experiment at a stirring speed of 300 rpm and room temperature. Then, the protein concentrations (mg/L) of both the feed (C_f) and permeate solution (C_p) were determined with a total organic carbon analyzer (TOC-VCPN, Shimadzu, Japan) at an operating pressure of 0.1 MPa for 2 h. The BSA rejection (R) was calculated with following equation:

$$R=\frac{C_f-C_p}{C_f}\times 100 \tag{3}$$

Hydrophilicity of the Blending System. The hydrophilicity of the membrane was evaluated on the basis of surface contact angle, equilibrium water content (EWC), and XPS analysis of the membranes.

The contact angles were measured with a contact angle meter (SL200C, Solon, China) at room temperature. Five microliters of water were dropped on the top surface of a dry membrane from a microsyringe with a stainless steel needle. The static contact angle was obtained by measurement of the average value of contact angles measured five times at different places on the membrane sample.

The EWC is related to the porosity of a membrane but indicates the hydrophilicity of a membrane. The membranes were swollen at 20°C for 12 h, and the free liquid on the top and bottom surfaces of the swollen membrane was padded dry with filter paper before it was weighed. Then, the weights of the wet and dry states of the membranes were measured with a moisture analyzer (DHS-16A, Qinghai, China), and the EWC was calculated with the following equation:

$$\mathrm{EWC}=\frac{G_{\mathrm{wet}}-G_{\mathrm{dry}}}{G_{\mathrm{wet}}}\times 100\% \tag{4}$$

In the previous formula, G_{dry} and G_{wet} represent the weights of the dry membrane and the swollen membrane in equilibrium with water (g), respectively.

The chemical compositions of the blend membrane surfaces were analyzed by XPS (PHI). The XPS experiments were carried out on an rapid beam deflector (RBD)-upgraded PHI-5000C ESCA system (PerkinElmer) with Mg Kα radiation [light quantum (E) = 1253.6 eV]. The X-ray anode was operated at 250 W, and the high voltage was kept at 14.0 kV with a detection angle of 54°. The binding energies were calibrated with carbon as a reference (C1s = 284.6 eV). The degree of PES-*g*-PEGMA surface enrichment (E) was calculated with eq. (5):[31]

$$E=\frac{A_{mo}}{A_{to}} \tag{5}$$

where A_{mo} is the atomic percentage of S on the blend membrane surface measured by XPS and A_{to} is the theoretical value of the S atomic percentage based on the total C, H, O, and S elements.

The degree of PES-*g*-PEGMA near-surface coverage (C) was calculated by the following equation:

$$C=\frac{A_{mo}}{A_{\mathrm{PES}-g-\mathrm{PEGMA}}}\times 100\% \tag{6}$$

where $A_{\mathrm{PES}\text{-}g\text{-}\mathrm{PEGMA}}$ is the atomic percentage of S of the PES-*g*-PEGMA material.

Tensile Strength and Elongation. The mechanical performance of the membranes was evaluated with a materials testing machine (H5K-S, United Kingdom) with a stretching rate of 20 mm/min at room temperature. Each specimen was cut into a 5 × 1 cm^2 piece, and the testing of each sample was repeated three times. The tensile extension and tensile strain at break were then measured to investigate the effect of the modification on the mechanical strength.

Fouling Resistance Measurement

The membrane-simulated crossflow,[32,33] realized by constant vigorous stirring in a dead-end filtration device connected with an air compressor pump and solution reservoir, was designed to characterize the filtration performance of the membranes. The membrane was first precompacted at a transmembrane pressure

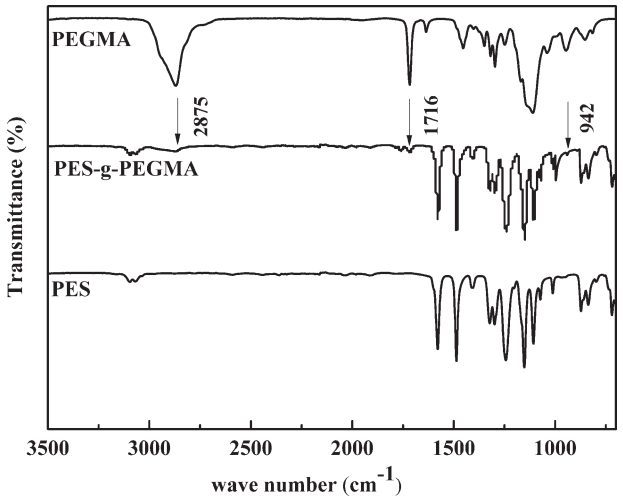

Figure 1. FTIR–ATR spectra of PES, PEGMA, and PES-*g*-PEGMA.

of 0.1 MPa with distilled water until a steady-state flux was observed. Then, the attenuation experiments were conducted with a BSA solution from an aeration tank as the feed needed to achieve quick and severe fouling on the membranes. The permeate flux of the BSA solution (J_{wB}) was also recorded at a constant transmembrane pressure of 0.1 MPa and room temperature for 300 min. Afterward, the membrane was dismounted from the cell, and the surface dirt was removed with a brush and sufficiently rinsed with running water. Afterward, a backwash was performed at a transmembrane pressure of 0.2 MPa for 15 min, and the after-cleaning pure water flux (J_{w2}) was measured in a similar way to that described earlier. The flux recovery ratio (FRR) was determined by the following equation:[29,34–36]

$$FRR = \frac{J_{w2}}{J_{w1}} \times 100\% \quad (6)$$

A higher FRR indicated preferable antifouling properties of the UF membranes.

To analyze the fouling process in detail, several resistance ratios were defined to describe the fouling resistance of the blend membranes.

The total fouling ratio (R_t), reversible fouling ratio (R_r), and irreversible fouling ratio (R_{ir}) were determined by the following equations:

$$R_t = 1 - \frac{J_{wB}}{J_{w1}} \times 100\% \quad (7)$$

$$R_r = \frac{J_{w2} - J_{wB}}{J_{w1}} \times 100\% \quad (8)$$

$$R_{ir} = \frac{J_{w1} - J_{w2}}{J_{w1}} \times 100\% \quad (9)$$

The ratio R_t is the sum of R_r and R_{ir}.

RESULTS AND DISCUSSION

FTIR–ATR Analysis of PES-*g*-PEGMA

To verify that the PEGMA monomer was grafted onto PES chains with benzoyl peroxide (BPO) as an initiator in the aqueous solution, PES flakes before and after modification were analyzed by FTIR–ATR spectroscopy. Figure 1 shows the respective IR spectra of PES, PEGMA, and PES-*g*-PEGMA. In a comparison of the IR spectra of the pure PES flakes and PEGMA, three new and significant absorbance bands at 2875, 1716, and 942 cm^{-1} were clear be seen in the IR spectra of PES-*g*-PEGMA. These bands were ascribed to the methyl (—CH_3), carbonyl (C═O), and ether (C—O—C) bond groups of PEGMA, respectively; this indicated the successful grafting of PEGMA onto PES.[37,38]

Compatibility of the PVC/PES-*g*-PEGMA Blend Membranes

The viscosity of the casting solutions can reveal the compatibility of blending systems. If the curve of the viscosity–constitution of the blending system is linear, the polymers are fully miscible. If the curve of the viscosity–constitution is nonlinear, the polymers are partial miscible. If the curve of the viscosity–constitution is an S segment, the polymers are fully immiscible.[39,40]

The viscosity–constitution curves of the PVC/PES-*g*-PEGMA and PVC/PES blending systems are shown in Figure 2, respectively. The curves of the viscosity–constitution of the PVC/PES-*g*-PEGMA and PVC/PES blending systems were both nonlinear, so the two blending systems were partial miscible. Additionally, the curve of the viscosity-constitution of the PVC/PES-*g*-PEGMA blending system tended to be more linear than that of PVC/PES system. This result indicates that the compatibility of the PVC/PES-*g*-PEGMA system was better than that of PVC/PES system. This may have been due to the interaction between the —PEGMA group and the element Cl.

The structures of the PVC/PES-*g*-PEGMA and PVC/PES membranes with blend ratios varying from 10 : 0 to 0 : 10 were studied by FTIR spectroscopy. Figure 3 shows the respective FTIR–ATR spectra for the top surface of membranes with different PVC/PES-*g*-PEGMA and PVC/PES ratios. In the FTIR spectrum of the pure PVC membrane, the absorbance at 2905 cm^{-1} corresponded to the stretching vibration peaks of C—H, the CH_2 deformation mode at 1426 and 1328 cm^{-1}, and the C—Cl stretching mode at 830 cm^{-1}. In a comparison of the IR spectra of these membranes, with increasing PES-*g*-PEGMA

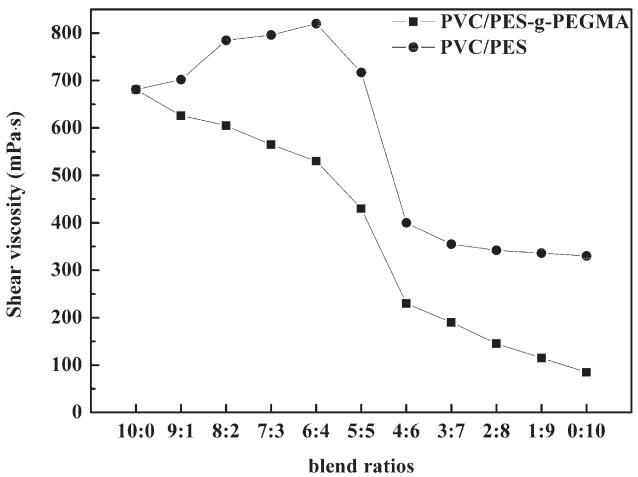

Figure 2. Shear viscosity of the PVC/PES-*g*-PEGMA and PVC/PES blending systems with different ratios.

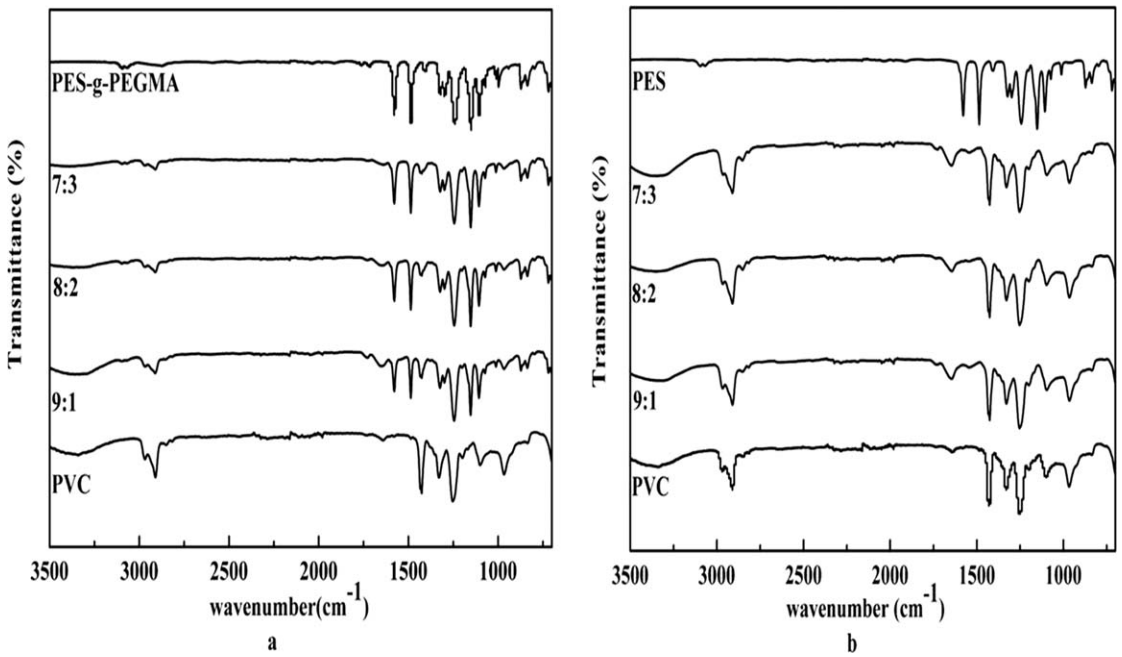

Figure 3. FTIR–ATR spectra of different amounts of the (a) PVC/PES-*g*-PEGMA and (b) PVC/PES membranes.

and PES content in the blending system, the deformation vibration peak at 2905 cm^{-1} of pure PVC membrane shifted to a higher frequency direction. These shifts were expected to be due to the antisymmetric C—H stretching vibration peaks at 3097 cm^{-1} of PES and to have a large impact on the symmetric C—H stretching of PVC at 2905 cm^{-1}. In addition to the shifts, when PVC was blended with PES-*g*-PEGMA, the C—H stretching of PVC at 2905 cm^{-1} was observed to decrease in intensity; this was attributed to the strong interaction between the symmetric C—H stretching of PVC at 2905 cm^{-1} and the methyl (—CH_3) stretching of PES-*g*-PEGMA at 2875 cm^{-1}. The CH_2 of PVC at 1426 and 1328 cm^{-1} were observed to have decreased in intensity as PES-*g*-PEGMA interacted with PVC. This confirmed the interaction between them. However, these trends were not obvious for the PVC/PES blending system. In addition, as with the PVC/PES-*g*-PEGMA blending system, the peak of PVC at 1328 cm^{-1} assigned to CH_2 shifted to the lower frequency direction because of the effect of hydrogen-bond formation between CH_2 and C—O—C on the stretching vibration peaks.[41–44]

As stated previously, these phenomena divulged that the PVC/PES-*g*-PEGMA blending system was partially compatible.[45] Furthermore, we concluded from the results that the interaction between the PVC and PES-*g*-PEGMA blending system was much stronger than that of the PVC and PES blending system and that PES-*g*-PEGMA exhibited better compatibility with PVC than with PES.

Membrane Structure and Morphology

The cross section and surface morphologies of the membranes were observed with SEM and FESEM, respectively.

The cross-sectional structures of the PVC/PES-*g*-PEGMA membranes at different blend ratios are displayed in Figure 4. The four photos all show typical asymmetric structures, dense skin layers, fingerlike porous sublayers, and spongelike bottom layers, which were due to the NIPS method. Interestingly, the membrane with a blend ratio of 9 : 1 tended to generate bigger fingerlike and denser spongelike pores. This may have been the result of the segregation of PES-*g*-PEGMA. With increasing PES-*g*-PEGMA content, the apertures of the fingerlike structures became larger, as shown in Figure 4(c,d). The spongelike

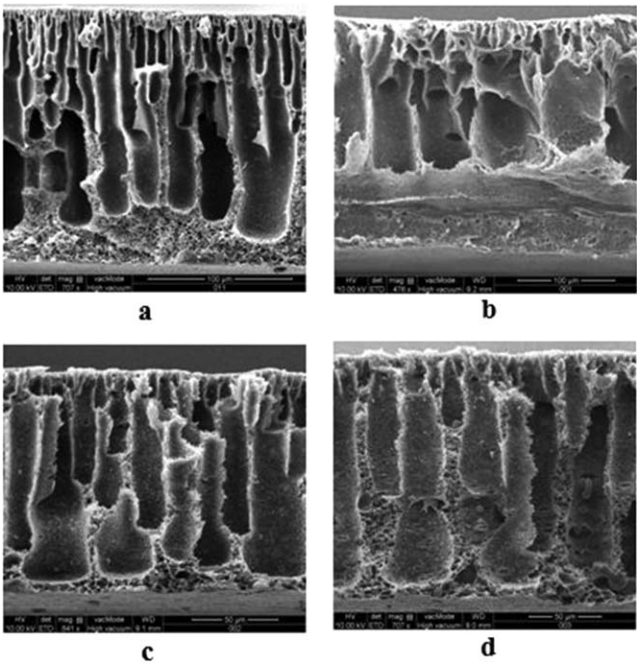

Figure 4. SEM cross-sectional images of the PVC/PES-*g*-PEGMA blending system with blend ratios of (a) 10 : 0, (b) 9 : 1, (c) 8 : 2, and (d) 7 : 3.

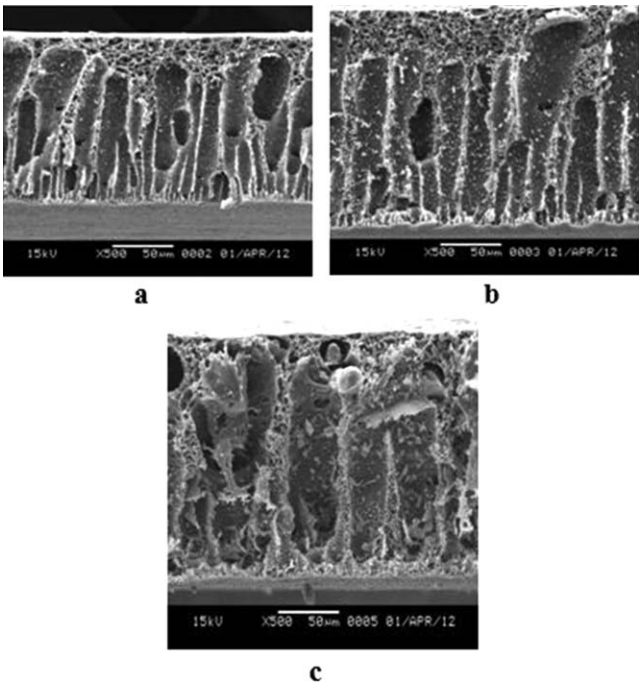

Figure 5. SEM cross-sectional images of the PVC/PES blending system with blend ratios of (a) 9 : 1, (b) 8 : 2, and (c) 7 : 3.

morphology of the membrane surface layer became thinner. Figure 5 shows the structures of the PVC/PES blend membranes. The skin layers of the PVC/PES blend membranes were denser than those of the PVC/PES-*g*-PEGMA blend membranes. This may have been because of the introduction of the hydrophilic PEGMA group in the PVC/PES-*g*-PEGMA blend membranes. The structures of the cross section of the PVC/PES blend membranes were also found to be more irregular than those of the PVC/PES-*g*-PEGMA blending system, as shown in Figures 4 and 5; this also implied that the PVC/PES-*g*-PEGMA blending system had better compatibility. Meanwhile, the number and size of pores on the membrane surfaces increased with increasing PES-*g*-PEGMA in the PVC/PES-*g*-PEGMA blending system, as shown in Figure 6.

Permeability and Rejection of the Blend Membranes

The effect of the blend ratio on the blend membrane performance was also investigated by pure water permeation and rejection. As shown in Table I, both the PVC/PES-*g*-PEGMA and PVC/PES blend membranes revealed the same phenomenon in which the pure water flux increased and the rejection decreased with decreasing PVC content.

The variation in the trend of pure water flux was attributed to the gradually larger fingerlike pores and thinner skin layers, which were caused by the increases in the PES-*g*-PEGMA and PES contents. The rejection relied more on the morphology of the skin layer than on the structure of the cross section. A comparison of the two different types of blend membranes revealed that the rejection and the pure water flux of the PVC/PES-*g*-PEGMA blend membranes were both close to those of the PVC/PES blend membranes. Table I also shows that all of the rejection values were higher than 80%; this indicated that the PVC/PES-*g*-PEGMA blending membranes were UF membranes that could be used not only in membrane biological reactors for wastewater treatment but also in pretreatment for the nanofiltration and reverse osmosis of drinking water, the concentration of proteins, and microbial clarification in the food and pharmaceutical industries.

Hydrophilicity of the PVC/PES-*g*-PEGMA Membranes

Figure 7 presents the water contact angles and EWC of the fabricated PVC filtration membranes with different PES-*g*-PEGMA contents. The pure PVC membrane had the biggest water contact angle of 70.29; this meant that it had the lowest hydrophilicity among the membranes. Furthermore, an increase in the content of PES-*g*-PEGMA in the membrane surface resulted in a decrease in the water contact angle. This meant that the hydrophilicity of the PVC/PES-*g*-PEGMA blending membranes was gradually enhanced. In addition, the EWC value increased from 66.7 to 84.6%; this was due to the increase in hydrophilicity and the number of pores in the membranes compared to the pure PVC membrane.

The surface components of the blend membranes were characterized by XPS analysis. Figure 8 illustrates four characteristic XPS signals for C, O, Cl, and S of the blend membranes. Figure 9 displays the changes in the peaks of O1s and S2p3 with different blend ratios. In Figure 9, it can be seen that the intensity of the O1s and S2p3 peaks both increased with the addition of PES-*g*-PEGMA. In addition, when the blend ratios were varied from 9 : 1 to 7 : 3, the O1s binding energy in the XPS spectra shifted from 537.6 to 538.6 eV. At the same time, the S2p3 binding energy increased slightly from 173.3 to 174.0 eV. This may have been due to an increase in the PES-*g*-PEGMA content on the membrane surface.

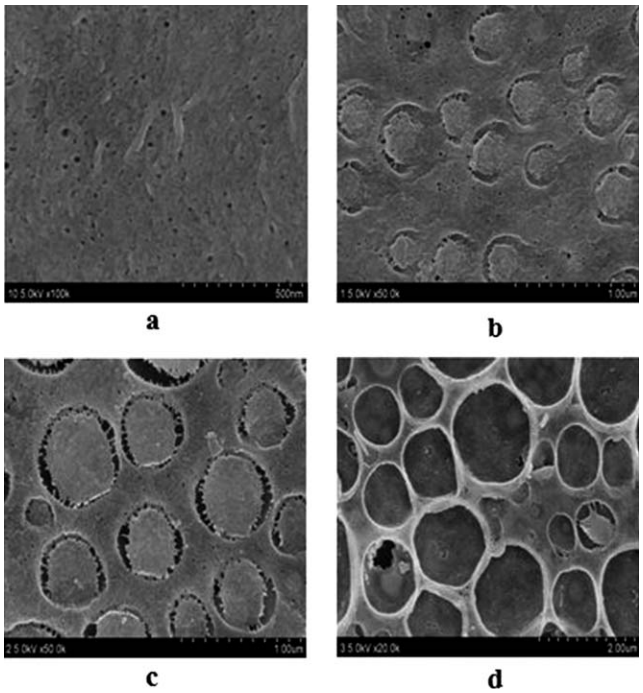

Figure 6. FESEM surface morphology images of the PVC/PES-*g*-PEGMA blending system with blend ratios of (a) 10 : 0, (b) 9 : 1, (c) 8 : 2, and (d) 7 : 3.

Table I. Measurements of the Pure Water Flux and Rejection of the PVC/PES-*g*-PEGMA and PVC/PES Membranes with Different Blend Ratios

		PVC/PES-*g*-PEGMA			PVC/PES		
	Pure PVC	9 : 1	8 : 2	7 : 3	9 : 1	8 : 2	7 : 3
Pure water flux (L m^{-2} h^{-1})	1.04	55.75	80.52	107.88	45.27	84.02	122.01
Rejection (%)	92.53	91.42	87.82	86.85	91.66	86.75	83.14

The membrane surface chemical compositions are illustrated in Table II. As shown clearly in Table II, the atomic percentages of the O and S elements on the membrane surfaces increased with increasing PES-*g*-PEGMA content in the membrane matrix. This phenomenon occurred because the hydrophilic segments of PES-*g*-PEGMA spontaneously segregated on the membrane surface when the casting film was immersed in the coagulant bath.[31,46] Additionally, with increasing PES-*g*-PEGMA content, the Cl element percentages on the PVC/PES-*g*-PEGMA blend membrane surfaces decreased from 24.78 to 16.70%; this indicated that the PVC content of the membrane surface dropped to some degree.

As shown in Table II, the values of *E* of the membranes decreased from 2.87 to 1.39 when the blend ratio was changed from 9 : 1 to 7 : 3. In contrast, the *C* values of the blend membranes increased gradually with increasing PES-*g*-PEGMA content in the membrane matrix. These phenomena revealed that the content of PES-*g*-PEGMA in the membrane surface was higher than in the membrane matrix because of the interaction between the hydrophilic groups and water molecules. This resulted in enhanced hydrophilicity in the blend membrane. This result was consistent with the measurements obtained for the water contact angle and EWC, as implied in Figure 7.

Mechanical Properties of the PVC/PES-*g*-PEGMA Blend Membranes

The mechanical properties of the PVC/PES-*g*-PEGMA blend membranes (with blend ratios varying from 10 : 0 to 7 : 3) are elucidated in Figure 10. Both the tensile strength and tensile elongation of the PVC/PES-*g*-PEGMA blend membranes (with blend ratios varying from 9 : 1 to 7 : 3) were lower than those of the pure PVC membranes. In the case of PES-*g*-PEGMA, there were more pores of larger size on the membrane; this led to a decreasing trend in the tensile strength and elongation. In addition, the partial compatibility of the blending system also played a role in the decline of the mechanical properties.

Antifouling Properties

Membrane fouling is mainly caused by the adsorption and deposition of proteins on the membrane surface and the entrapment of proteins in the pores. Membrane fouling consists of reversible and irreversible fouling. Reversible fouling allows water flux recovery and can be removed by simple hydraulic cleaning. Irreversible fouling is responsible for any observed decrease in the flux of pure water before and after the filtration of a BSA solution and is due to the strong adsorption of BSA molecules on the surface or entrapment of BSA molecules in pores.[29,47]

The change in FRR is shown in Figure 11. As shown in Figure 11, the water flux declined gradually and then reached a stable value; this may have been because of the large pore diameters and fingerlike structures of the PVC/PES-*g*-PEGMA membranes, which tended to become plugged. With increasing content of PES-*g*-PEGMA, the PVC/PES-*g*-PEGMA blend membrane had a higher steady-state flux for overall long-term application, and as a consequence of pore formation and hydrophilicity enhancement, the flux increased significantly. Additionally, after backwashing, the cleaned membranes were evaluated by the pure water flux at steady state. This evaluation showed that the fluxes did not recover to their original values because of irreversible fouling on the membrane surface. Interestingly, all of the blend membranes' permeate flux values of BSA solution were lower than the pure water flux for the increased feed concentration as

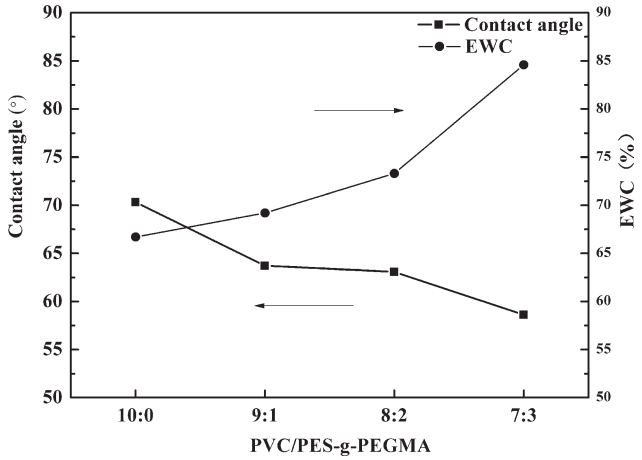

Figure 7. Measurement of the contact angles and EWC of PVC/PES-*g*-PEGMA blend membranes.

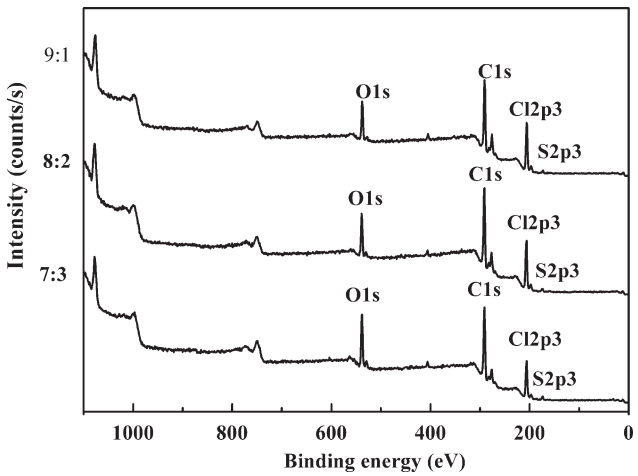

Figure 8. XPS analysis results for the PVC/PES-*g*-PEGMA blend membranes.

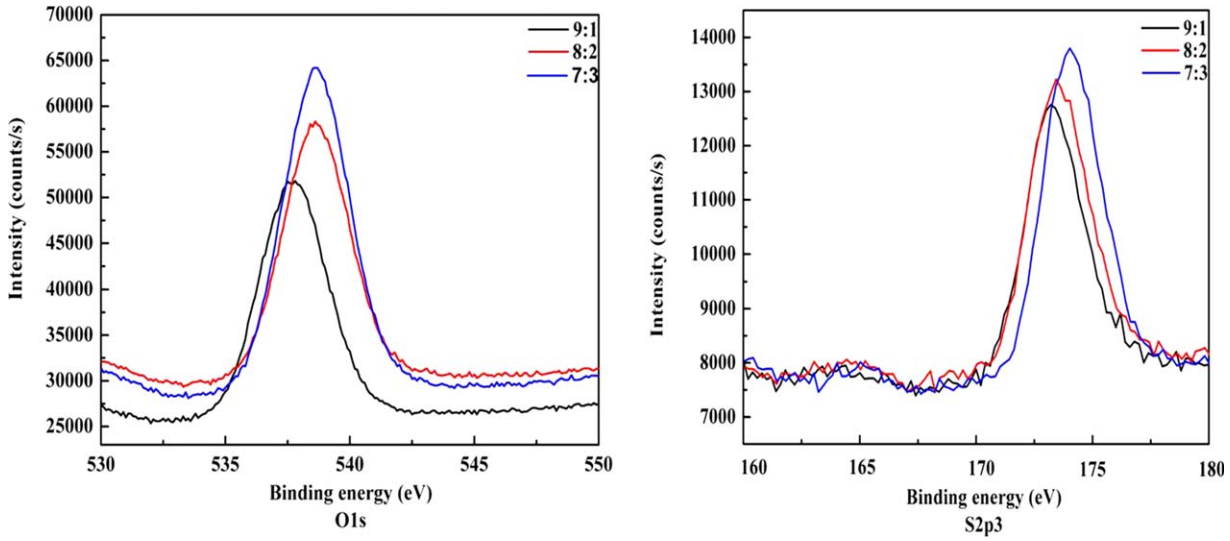

Figure 9. O1s and S2p3 core-level XPS spectra of the PVC/PES-*g*-PEGMA blend membranes with PES-*g*-PEGMA as an additive. [Color figure can be viewed in the online issue, which is available at wileyonlinelibrary.com.]

a result of the removal of the permeate and the increased hydraulic resistance of the gel layer formed on the membrane surface.

The antifouling properties of the PVC/PES-*g*-PEGMA membranes with different blend ratios were calculated and are summarized in Table III. With increasing PES-*g*-PEGMA content, the FRR values of the blend membranes increased and the R_t values decreased, but within the R_t values, the R_r values of the blend membranes increased, and the R_{ir} values decreased when the blend ratio varied from 9 : 1 to 7 : 3. This result indicated that the blend membranes had better antifouling properties than the pure PVC membranes; this was due to the improvement of the blend membrane hydrophilicity. So, we concluded that membranes prepared with the addition of hydrophilic modifiers had a higher resistance to fouling than those without modifiers, and a greater content of PES-*g*-PEGMA produced superior antifouling properties. The optimum blend ratio of the PVC/PES-*g*-PEGMA blend membranes was 7 : 3.

CONCLUSIONS

PEGMA was grafted onto PES by a simple and effective method with BPO as an initiator and was then blended with PVC with the NIPS method to fabricate PVC/PES-*g*-PEGMA blend membranes. The UF performance and fouling resistance of these membranes were investigated, and the following conclusions were drawn:

1. The FTIR–ATR results revealed that the interaction between the PVC and PES-*g*-PEGMA blending systems was much stronger than that of PVC and PES blending systems. Both the results of FTIR–ATR spectroscopy and shear viscosity measurements showed that PES-*g*-PEGMA had better compatibility with PVC than did PES and that the PVC/PES-*g*-PEGMA blending system was partially miscible.
2. SEM analysis of the PVC/PES-*g*-PEGMA and PVC/PES blend membranes revealed asymmetrical fingerlike structures. The wall of the fingerlike pore was spongelike. The addition of PES-*g*-PEGMA or PES created larger apertures in the fingerlike structures and thinner spongelike morphologies of the membrane surface layers. The results of FESEM indicated that the surface pores of the blend membranes became bigger and that the pore number increased as the PES-*g*-PEGMA content was increased. Meanwhile, all of the

Table II. Experimental Values of the Membrane Surface Chemical Composition, Degree of PVC/PES-*g*-PEGMA *E*, and *C*

PVC/PES-*g*-PEGMA	C1s (%)	O1s (%)	Cl 2p3 (%)	S2p3 (%)	*E*	*C* (%)
10 : 0	75.22	0	24.78	0	0	0
9 : 1	71.44	8.10	19.35	1.10	2.87	28.95
8 : 2	70.42	10.13	17.30	2.15	2.27	56.14
7 : 3	69.48	11.28	16.70	2.27	1.39	59.27

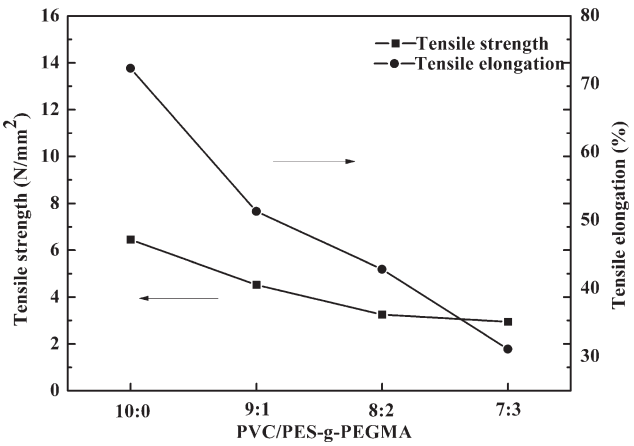

Figure 10. Measurements of the tensile strength and tensile elongation of the PVC/PES-*g*-PEGMA blend membranes.

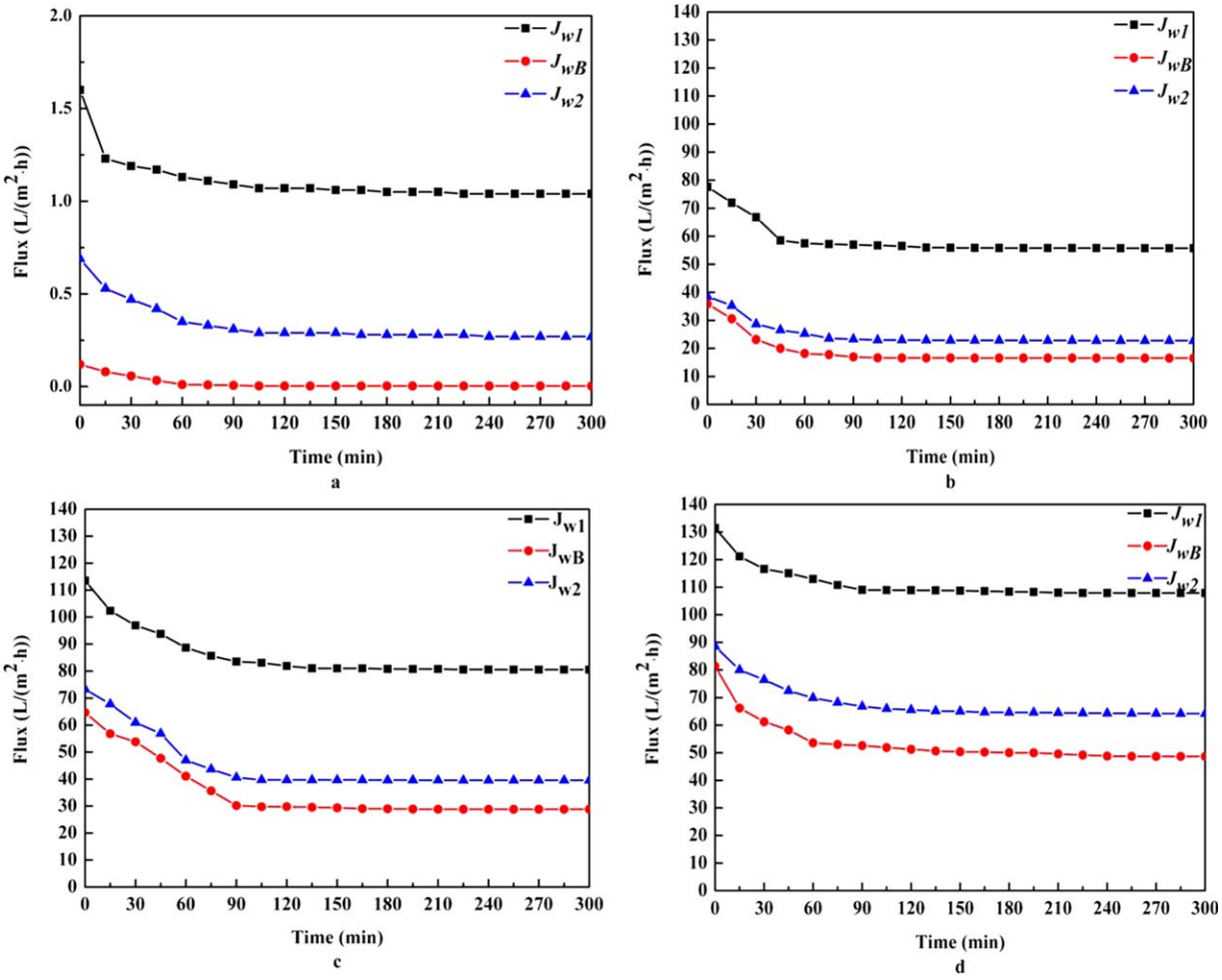

Figure 11. Flux behavior of the PVC/PES-*g*-PEGMA membranes with blend ratios of (a) 10 : 0, (b) 9 : 1, (c) 8 : 2, and (d) 7 : 3. [Color figure can be viewed in the online issue, which is available at www.interscience.wiley.com.]

blend membranes showed higher fluxes than the pure PVC membrane but exhibited lower rejection because of their membrane structures and morphologies.

3. The hydrophilicity of the blend membranes was improved. When PES-*g*-PEGMA was added to PVC, the contact angle of the PVC membranes decreased, and the EWC increased as a result of the larger pore size of the membranes compared to that of the pure PVC membranes. The enrichment of the PES-*g*-PEGMA segments on the membrane surface was confirmed by XPS and led to enhanced hydrophilicity in the PVC/PES-*g*-PEGMA blend membranes. The decline in the tensile strength and elongation of the PVC/PES-*g*-PEGMA blend membranes (with blend ratios varying from 9 : 1 to 7 : 3) was mainly caused by the macrovoids.
4. The fouling resistance measurements indicated that the PVC/PES-*g*-PEGMA membranes (with blend ratios varying from 9 : 1 to 7 : 3) had higher resistance than the pure PVC membranes, and with increasing PES-*g*-PEGMA content, the PVC/PES-*g*-PEGMA membranes exhibited superior antifouling properties. The optimum blend ratio of the PVC/PES-*g*-PEGMA blend membranes was found to be 7 : 3.

Table III. Antibiofouling Properties of the PVC/PES-*g*-PEGMA Membranes with Different Blend Ratios

PVC/PES-*g*-PEGMA	FRR (%)	R_t (%)	R_r (%)	R_{ir} (%)
10 : 0	25.96	99.71	25.67	74.04
9 : 1	40.81	70.39	11.20	59.19
8 : 2	49.11	64.21	13.32	50.89
7 : 3	59.52	54.88	14.40	40.48

REFERENCES

1. Gao, Y.; Haavisto, S.; Tang, C. Y.; Salmela, J.; Li, W. *J. Membr. Sci.* **2013**, *448*, 198.
2. Lewis, R.; Nothrop, S.; Chow, C. W. K.; Everson, A.; Leeuwen, J. A. V. *Sep. Purif. Technol.* **2013**, *114*, 1.
3. Saboyainsta, L. V.; Maubois, J. L. *Lait* **2000**, *80*, 541.
4. Le-Clech, P.; Chen, V.; Fane, T. A. G. *J. Membr. Sci.* **2006**, *284*, 17.
5. Cath, T. Y.; Gormly, S.; Beaudry, E. G.; Flynnc, M. T.; Adamsa, V. D.; Childressa, E. A. *J. Membr. Sci.* **2005**, *257*, 85.

6. Santos, E. B. H.; Duarte, R. M. B. O.; Filipe, O. S.; Duarte, A. C. *Int. J. Environ. Anal. Chem.* **2000**, *78*, 333.
7. Lindström-Seppä, P.; Huuskonen, S.; Kotelevtsev, S.; Mikkelson, P.; Raanen, T.; Stepanova, L.; Stepanova, L.; Hanninen, O. *Mar. Environ. Res.* **1998**, *46*, 273.
8. Cornelissen, E. R.; Harmsen, D.; De Korte, K. F.; Ruiken, C. J.; Qin, J. J.; Oo, H.; Wessels, L. P. *J. Membr. Sci.* **2008**, *319*, 158.
9. Kitaura, T.; Fadzlina, W. N.; Ohmukai, Y.; Maruyama, T.; Matsuyama, H. *J. Appl. Polym. Sci.* **2013**, *127*, 4072.
10. Chiang, Y. C.; Chang, Y.; Higuchi, A.; Chen, W. Y.; Ruaan, R. C. *J. Membr. Sci.* **2009**, *339*, 151.
11. Chan, R.; Chen, V. *J. Membr. Sci.* **2004**, *242*, 169.
12. Hosseini, S. M.; Madaeni, S. S.; Zendehnam, A.; Moghadassi, A. R.; Khodabakhshi, A. R.; Sanaeepur, H. *J. Ind. Eng. Chem.* **2013**, *19*, 854.
13. Xu, J.; Wang, J.; Luo, W. *Membr. Sci. Technol.* **2011**, *31*, 1.
14. Ulutan, S.; Balköse, D. *J. Membr. Sci.* **1996**, *115*, 217.
15. Peng, Y.; Sui, Y. *Desalination* **2006**, *196*, 13.
16. Mei, S.; Xiao, C.; Hu, X.; Shu, W. *Desalination* **2011**, *280*, 378.
17. Alsalhy, Q. F. *Desalination* **2012**, *294*, 44.
18. Sohbatzadeh, F.; Mirzanejhad, S.; Ghasemi, M.; Talebzadeh, M. *J. Electrostat.* **2013**, *71*, 875.
19. Li, W.; Yuan, M.; Yang, M. *Eur. Polym. J.* **2006**, *42*, 1396.
20. Bigot, S.; Louarn, G.; Kébir, N.; Burel, F. *Carbohydr. Polym.* **2013**, *98*, 1644.
21. Bigot, S.; Louarn, G.; Kébir, N.; Burel, F. *Appl. Surf. Sci.* **2013**, *283*, 411.
22. Wu, P.; Zhang, L. Polymer Blending Modification; China Light Industry: Beijing, **1996**; p 1.
23. Su, Y.; Li, C.; Zhao, W.; Shi, Q.; Wang, H.; Jiang, Z.; Zhu, S. *J. Membr. Sci.* **2008**, *322*, 171.
24. Wang, Y.; Su, Y.; Sun, Q.; Ma, X.; Ma, X.; Jiang, Z. *J. Membr. Sci.* **2006**, *282*, 44.
25. Rahimpour, A.; Madaeni, S. S. *J. Membr. Sci.* **2007**, *305*, 299.
26. Madaeni, S. S.; Pourghorbani, R. *Adv. Polym. Technol.* **2013**, *32*, 141.
27. Shi, Q.; Su, Y.; Ning, X.; Ning, X.; Chen, W.; Peng, J.; Jiang, Z. *J. Membr. Sci.* **2010**, *347*, 62.
28. Yune, P. S.; Kilduff, J. E.; Belfort, G. *J. Membr. Sci.* **2011**, *370*, 166.
29. Peng, J.; Su, Y.; Shi, Q.; Chen, W.; Jiang, Z. *Bioresour. Technol.* **2011**, *102*, 2289.
30. Makhlouf, C.; Marais, S.; Roudesli, S. *Appl. Surf. Sci.* **2007**, *253*, 5521.
31. Mu, C.; Su, Y.; Sun, M.; Chen, W.; Jiang, Z. *J. Membr. Sci.* **2010**, *350*, 293.
32. Sim, L. N.; Ye, Y.; Chen, V.; Fane, A. G. *J. Membr. Sci.* **2010**, *360*, 174.
33. Koo, C. H.; Mohammad, A. W.; Suja, F.; Talib, M. Z. M. *J. Membr. Sci.* **2013**, *435*, 165.
34. Xu, J.; Feng, X.; Hou, J.; Wang, X.; Shan, B. T.; Yu, L. M.; Gao, C. J. *J. Membr. Sci.* **2013**, *446*, 171.
35. Daraei, P.; Madaeni, S. S.; Ghaemi, N.; Khadivi, M. A.; Astinchap, B.; Moradian, R. *Sep. Purif. Technol.* **2013**, *109*, 111.
36. Chen, W.; Su, Y.; Zhang, L.; Shi, Q.; Peng, J.; Jiang, Z. *J. Membr. Sci.* **2010**, *348*, 75.
37. Liu, F.; Du, C. H.; Zhu, B. K.; Xu, Y. Y. *Polymer* **2007**, *48*, 2910.
38. Hashim, N. A.; Liu, F.; Li, K. *J. Membr. Sci.* **2009**, *345*, 134.
39. Kuleznev, V. N.; Melnikova, O. L.; Klykova, V. D. *Eur. Polym. J.* **1978**,*14*, 455.
40. Singh, Y. P.; Singh, R. P. *Eur. Polym. J.* **1983**, *19*, 535.
41. Ramesh, S.; Yi, L. *J. Ionics* **2009**, *15*, 413.
42. Li, W.; Yuan, M.; Yang, M. *Eur. Polym. J.* **2006**, *42*, 1396.
43. Zhao, J.; Wang, X.; Zhou, W.; Zhi, E.; Zhang, W.; Ji, J. *J. Appl. Polym. Sci.* **2013**, *130*, 3212.
44. Prasath, M.; Muthu, S.; Arun Balaji, R. *Spectrochim. Acta A* **2013**, *113*, 224.
45. Li, Y. Research of Solution Blending in Modification of PVDF Membrane; Donghua University: Shanghai, **2012**.
46. Yokoyama, H.; Miyamae, T.; Han, S.; Ishizone, T.; Tanaka, K.; Takahara, A.; Torikai, N. *Macromolecules* **2005**, *38*, 5180.
47. Pieracci, J.; Crivello, J. V.; Belfort, G. *J. Membr. Sci.* **2002**, *202*, 1.